Marriage of XAFS and crystallography for structure–function studies of metalloproteins

S. Samar Hasnain* and Richard W. Strange

College of Biology and Medicine, CLRC Daresbury Laboratory, Warrington WA4 4AD, UK. E-mail: s.hasnain@dl.ac.uk

Metalloproteins constitute a significant proportion of all known genomes. In this article it is shown that the marriage of two synchrotron-radiation-based structural techniques, namely high-resolution crystallography and XAFS, can yield unprecedented levels of structural information that is directly relevant to the mechanism/function of these important macromolecules.

Keywords: metalloproteins; genomes; high-resolution crystallography; XAFS.

1. Introduction

Detailed structural data for the metal sites in a metalloprotein, at a resolution commensurate with their chemical properties, are essential if the sites' functional role in the metalloprotein is to be fully understood. The structural changes to the metal coordination during redox or substrate-binding reactions are generally at ≤ 0.1 Å, and EXAFS is an ideal structural technique for defining these subtle changes. The accuracy of metal centres defined by EXAFS is comparable to that of small-molecule crystal structures and is far superior to that of most protein crystal structures, where the resolution is ~1.5 Å or less. Protein crystal structure determinations at atomic (or better) resolution† are capable of defining the metal sites to a sufficient accuracy and resolution to determine these effects, and advances in synchrotron sources and detectors are now enabling atomic-resolution data to be obtained in an increasing number of cases. However, the number of such structures remains a small fraction of the total. For example, there are no true atomic-resolution structures among the 200 or so structures of copper proteins in the PDB.‡ Advances have also taken place in the X-ray absorption method in recent years, such as the availability of superior X-ray fluorescence detectors, the use of sagittal focusing optics and important theoretical developments, all of which have allowed high-quality EXAFS data to be measured on samples with low metal content and then analysed more rigorously than in the past.

We have demonstrated that the combination of high-resolution crystallographic information and ultra-high-resolution EXAFS is a powerful approach for studying the structure–function relationships in proteins, particularly when subtle structural changes are associated with a chemical reaction (Cheung *et al.*, 2000). This approach, which makes direct use of three-dimensional information from protein crystal structures in the analysis of EXAFS data, is likely to be of most interest in cases where crystallographic information is available for some state of a protein but not for others; for example, the resting-state structure may be known but crystallographic data on reactive intermediates may be lacking. In such circumstances EXAFS data on different states of the protein may be solved by the combined approach in order to predict structural changes and to examine how these intermediate states perturb the metal at the catalytic site. The combined approach can also be used in a more straightforward manner to enhance the details of the metal environment provided by the protein crystal structure. The approach can be applied regardless of the crystal structure resolution (at least up to 3.5 Å), and we give an example below that uses three different sets of coordinates for a Cu-containing nitrite reductase, which are measured between 1.04 and 3.0 Å resolution. We show that there is excellent agreement between the PX and XAFS models for the Cu sites for atomic-resolution structures but that agreement is much worse at the lower resolutions. This result further highlights the importance of atomic-resolution crystal structure data for investigating the subtle structural changes that accompany chemical activity.

Another aspect that brings a significant link between protein crystallography and EXAFS is in the determination of oxidation states at metal centres. We would recommend, where technically possible, that all metalloprotein crystallography data collection is accompanied by on-line edge measurements, or at least 'before-and-after' measurements of the absorption edges of the metals involved, so that oxidation states of the protein to which the crystallographic structure corresponds can be ascertained. X-ray-induced reduction of metals is a significant problem for advanced synchrotron radiation sources. Whether a metalloprotein contains oxidized, reduced or mixed metal oxidation states, and whether these might be due to photoreduction, to a natural feature of the protein or to crystallization conditions, are all possibilities that need to be addressed. In this paper we present an example where EXAFS and protein crystallography work together to resolve such a problem for CuZn bovine superoxide dismutase.

2. The type 2 Cu site of AxNiR

Dissimilatory copper nitrite reductases (NiRs) play an essential role in the cycling of nitrogen in the biosphere, catalysing the reaction $NO_2^- + 1e^- + 2H^+ \rightarrow NO + H_2O$ (Zumpft, 1997). In addition to its importance in microbial bioenergetics, this process has environmental impact in generating N_2O, which is a potent greenhouse gas, and in removing polluting nitrate from groundwater. The conversion of nitrite to nitric oxide, catalysed by dissimilatory nitrite reductases, is a key step in denitrification, since this reaction is the point at which fixed nitrogen in the soil is converted to a gaseous product, which can result in significant losses of nitrogen to the atmosphere.

The highly homologous family of Cu-containing nitrite reductases are of two subclasses, which are either blue or green depending on the bacterial species from which they are isolated. Crystallographic structures of both subclasses have been reported (Dodd *et al.*, 1997, 1998; Godden *et al.*, 1991; Kokimota *et al.*, 1994; Adman *et al.*, 1995; Murphy, Turley & Adman, 1997; Murphy *et al.*, 1995) and demonstrate that these enzymes are trimers.

Both classes of enzyme contain type 1 and type 2 Cu centres in each monomer, with the type 2 Cu situated in the intermonomer cleft. Spectroscopic and structural studies on oxidized NiRs have led to the view that the type 2 Cu binds nitrite and that electron transfer to the type 2 Cu from reduced azurin or pseudoazurin is mediated *via* the type 1 Cu site, which lies ~4 Å from the protein surface. In *Alcaligenes xylosoxidans* NiR (AxNiR) the two Cu atoms are separated by 12.6 Å and are connected directly through residues Cys130 and His129, which are ligands to the type 1 and type 2 Cu atoms, respectively. X-ray crystal structure data (Dodd *et al.*, 1997), together with ENDOR (electron nuclear double resonance) (Howes *et al.*, 1994) and EXAFS (Strange *et al.*, 1995) studies of AxNiR, have

† Atomic resolution in protein crystallography (PX) is taken to be 1.2 Å, the distance at which C—C bonds may be resolved.

‡ We have recently determined a number of structures (as yet unpublished) at these resolutions for copper proteins. The present article takes account of what we know from these structures.

shown that, in the presence of substrate, a water bound to the type 2 Cu in the oxidized form of the enzyme is replaced by a nitrite molecule.

The availability of AxNiR deficient in type 2 copper (T2DNiR) has allowed us to investigate the structures of the two types of copper sites in this enzyme through the use of the difference EXAFS technique. We were able to define the changes that take place when the Cu atoms are reduced and when substrate–ligand binding occurs (Strange *et al.*, 1995, 1999), and on this basis an ordered catalytic mechanism for nitrite reduction (Strange *et al.*, 1999) was established.

The crystal structures of native AxNiR at 3.0 Å (1NDR.PDB; Dodd *et al.*, 1997), 1.9 Å (1HAU.PDB; Ellis *et al.*, 2001) and 1.04 Å (Ellis *et al.*, 2003) resolutions and the nitrite-bound complex of AxNiR at 2.8 Å resolution (1NDS.PDB; Dodd *et al.*, 1997) were used to give starting models for the refinement of the corresponding solution XAFS data. This refinement was performed with the *EXCURVE* program (Binsted *et al.*, 1991, 1992; Binsted & Hasnain, 1996).

2.1. The crystal structures of native and nitrite-bound proteins

The type 2 Cu site lies in a ∼13 Å-deep cleft between domain I and domain II of adjacent monomers, where the Cu is directly exposed to the solvent. This copper is ligated by His94 and His129 from domain I of one monomer and by His300 from domain II of the adjacent monomer. In addition, there is a water molecule coordinated to the copper (Fig. 1*a*). In the nitrite-bound form, this water is replaced by a nitrite ligand that binds in a bidentate fashion (Fig. 1*b*). The Cu–

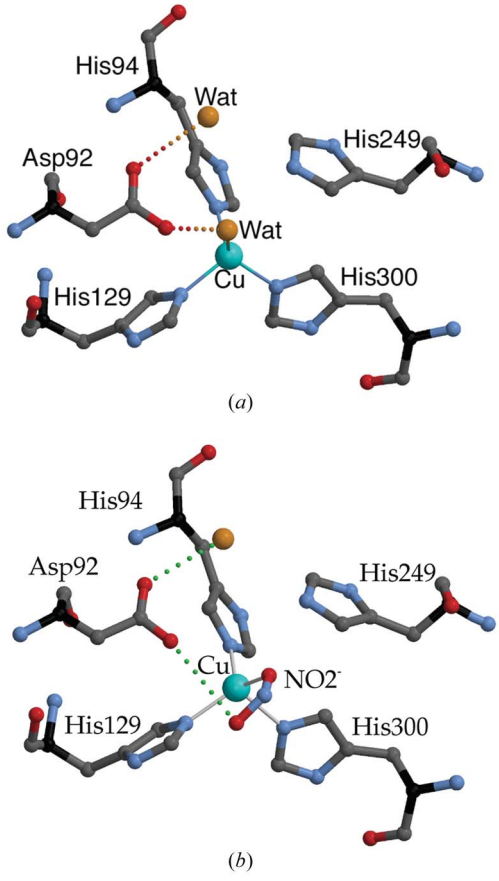

Figure 1
Coordination of (*a*) the native oxidized type 2 Cu site of native AxNiR, (*b*) the nitrite-bound type 2 Cu site (Dodd *et al.*, 1997).

Table 1
Cu–ligand distances (in Å) from oxidized AxNiR crystal structures at different resolutions and from two-dimensional solution EXAFS.

	Native protein				Nitrite derivative	
	PX			EXAFS	PX	EXAFS
Resolution (Å)	3.0	1.9	1.04	–	2.8	–
His94	2.08	2.02	1.96	1.95	2.12	2.03
His129	2.09	2.04	1.99	1.95	1.99	2.03
His300	1.96	2.26	1.90	1.95	2.09	2.03
Water	1.70	1.71	1.95	1.98	–	–
Nitrite (O1)	–	–	–	–	1.73	1.95
Nitrite (O2)	–	–	–	–	2.48	2.85
Reference	Dodd *et al.* (1997)	Ellis *et al.* (2001)	Ellis *et al.* (2003)	Strange *et al.* (1995)	Dodd *et al.* (1997)	Strange *et al.* (1995)

ligand distances for these structures, which are solved between 3.0 Å and 1.04 Å resolution, are summarized in Table 1. The 1.04 Å data for the native enzyme was obtained from frozen crystals using polyethylene glycol (PEG) and do not yield to nitrite soaking. The nitrite-bound room-temperature data were obtained from crystals grown without PEG. This restriction has so far prevented improvements in data resolution of the nitrite form. EXAFS has therefore been used to provide a means of examining the nature of nitrite binding at much higher resolution than is available crystallographically.

2.1.1. EXAFS of the oxidized native protein. Theoretical Cu *K*-edge EXAFS spectra, which we calculated using the crystallographic coordinates from the three PDB files 1NDR, 1HAU and 1ELLIS, are compared in Fig. 2 with the experimental k^3-weighted EXAFS spectrum of the oxidized type 2 Cu site. The curve calculated from the 1.04 Å-resolution crystal structure is in excellent agreement (fit index 0.65) with the experimental spectrum (Fig. 2*c*) and is clearly superior to the simulations obtained with the coordinates of the medium- (fit index 5.4) and low-resolution (fit index 6.3) structures. Table 1 provides the explanation for this fact: the water molecule is placed at 1.7 Å from the type 2 Cu in both of the lower-resolution structures, whereas it is at the chemically more reasonable distance of 1.95 Å in the atomic-resolution structure. Furthermore, the three histidine ligands are shorter by ∼0.1 Å. The atomic-resolution crystal structure Cu–ligand distances are also in good agreement with our earlier solution EXAFS study of AxNiR, which preceded the first 3.0 Å-resolution crystal structure of this protein (Strange *et al.*, 1995). This example shows that solution state EXAFS yields accurate metrical information comparable to that obtained by atomic resolution crystallography.

2.1.2. EXAFS of the nitrite derivative. At 2.8 Å resolution, the crystal structure of the nitrite derivative of AxNiR (Dodd *et al.*, 1997) provides a poor fit (fit index 4.6) to the EXAFS spectrum of the nitrite-bound type 2 Cu site, as shown in Fig. 3. The parameters of the earlier two-dimensional EXAFS simulation (Strange *et al.*, 1995), which are listed in Table 1, show that significant shifts in the Cu–ligand distances are required to obtain the best fit to the data. The refined Cu—N(histidine) distances and the much longer (by 0.2 Å) Cu—O1(nitrite) distances that are obtained from this two-dimensional EXAFS study provided the main improvement in the fit to the experimental spectrum. It was not clear from this earlier study whether or not the nitrite ligand was bound to Cu in a bidentate fashion. In the present study we have used the three-dimensional information provided by the crystal structure to reexamine the mode of binding of the nitrite group. First, the Cu—N(histidine) distances

were set to 2.03 Å, as in the two-dimensional EXAFS study (giving a fit index of 3.0). Then, a two-dimensional least-squares contour map was calculated by the variation of the distance Cu—O1(nitrite) and the angle Cu—O1(nitrite)—O2(nitrite) over a given set of ranges (Fig. 4). This gave two minima: one corresponds to a bidentate mode of binding for the nitrite ligand, with Cu—O1 and Cu—O2 distances of 1.94 Å and 2.32 Å, respectively (fit index 0.98); the best minimum occurred for a monodentate form of binding, similar to that found in the earlier two-dimensional EXAFS study, with a Cu—O1 distance of 1.94 Å and a Cu—O2 distance of 2.98 Å (fit index 0.87). These are compared with the crystal structure in Fig. 5.

3. The Cu centre of bovine CuZn superoxide dismutase

CuZn superoxide dismutase, CuZnSOD, catalyses the dismutation reaction of the toxic superoxide radical ($O_2^{\bullet -}$) to molecular oxygen and hydrogen peroxide and thus forms a crucial part of the cellular antioxidant defence mechanism:

$$\text{SOD-Cu}^{2+} + O_2^{\bullet -} \rightarrow \text{SOD-Cu}^{1+} + O_2,$$

$$\text{SOD-Cu}^{1+} + O_2^{\bullet -} + 2H^+ \rightarrow \text{Enz-Cu}^{2+} + H_2O_2.$$

SODs are enzymes with medical relevance as potential therapeutic agents in diseases related to oxidative stress and play a role in moderating the ageing process. Single-point mutations in SOD are associated with the development of a form of motor neuron disease.

CuZnSOD is a dimer of molecular weight 32 KDa. Each 151 amino acid monomer folds as an eight-stranded 'greek-key' β-barrel connected by three external loops (Tainer *et al.*, 1982) (Fig. 6*a*). The three-dimensional structure of CuZnSOD in the Cu(II) form has been well established by a number of X-ray crystallographic studies (Tainer *et al.*, 1983; Djinovic *et al.*, 1992) and is strongly conserved across eukaryotic species (Bordo *et al.*, 1994).

The active site of bovine SOD (CuZnBSOD) lies at the base of a 15 Å-deep cavity formed by two loops. These loops contain charged residues that facilitate the electrostatic guidance of superoxide to the active site. The active site of the oxidized, Cu(II), enzyme consists of

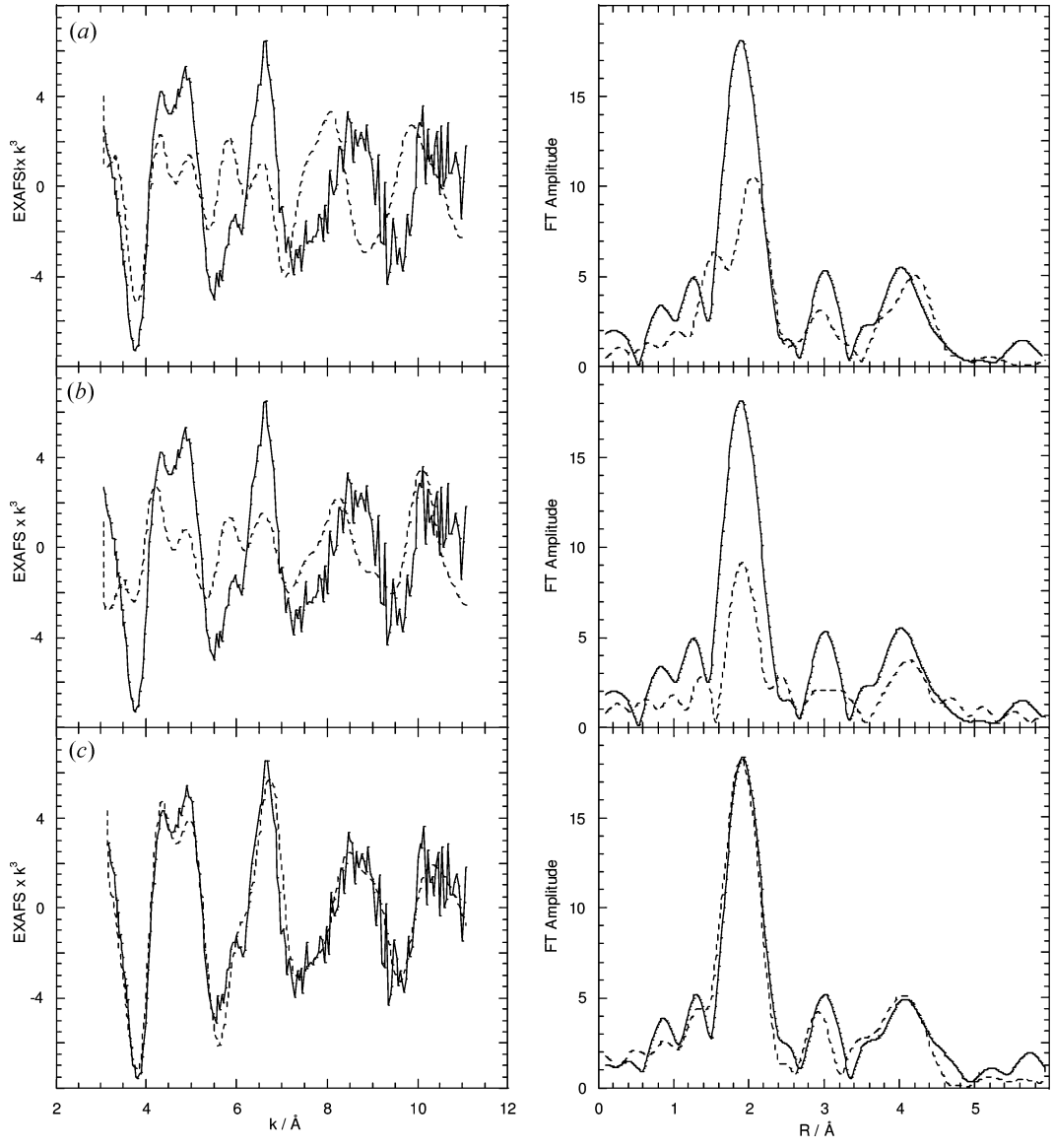

Figure 2
The k^3-weighted K-edge EXAFS spectrum of the type 2 Cu site of AxNiR and three simulations (dashed lines) calculated using crystallographic data at (*a*) 3.0 Å (1NDR.PDB), (*b*) 1.9 Å (1HAU.PDB) and (*c*) 1.04 Å resolution.

one copper and one zinc ion bridged by the imidazole ring of histidine 61, a feature unique to enzymes of this class. The Cu is coordinated by a further three histidine ligands and a water molecule, while Zn is ligated by two additional histidines and an aspartic acid (Fig. 6*b*).

The generally accepted mechanism of catalysis for the CuZnSODs (Tainer *et al.*, 1983) involves the cyclic reduction and reoxidation of Cu by successive molecules of superoxide.

In this mechanism, on reduction of Cu(II) by the superoxide anion, His61 becomes dissociated from Cu and is protonated, and the coordinated water molecule is displaced; a three-coordinate Cu(I) site is thus produced (Tainer *et al.*, 1983). Cu is then reoxidized by a second molecule of superoxide *via* proton donation from His61 and from the solvent, and hydrogen peroxide is released. The key feature of this mechanism is the transition from five-coordinate Cu to three-coordinate Cu on reduction of the metal ion. XAFS demonstrated the existence of a three-coordinate Cu(I) site in bovine SOD (Blackburn *et al.*, 1984) a decade before the first crystallographic attempt to determine the structure of the reduced protein (Rypniewski *et al.*, 1995). This determination actually reported a five-coordinate Cu site for the reduced bovine enzyme, but this result has not been supported by more recent crystal structures (Ogihara *et al.*, 1996; Hart *et al.*, 1998; Hough & Hasnain, 1999), which have tended to show a three-coordinate Cu(I) coordination that is consistent with the earlier biochemical (McAdam *et al.*, 1977) and NMR (Bertini *et al.*, 1992) and further EXAFS (Murphy, Strange & Hasnain, 1997) studies. The strongest evidence for the break of the His61 imidazole bridge in the reduced crystalline protein has been supplied by an XAFS study of protein crystals (Ascone *et al.*, 1997). These XAFS studies taken together provide a strong case in favour of the 'Tainer' reaction mechanism.

These studies have also highlighted the difficulty of obtaining a particular oxidation state during protein crystallography experiments. We recently reported a crystallographic study of bovine SOD carried out at the SRS Daresbury Laboratory in which one subunit contained a three-coordinate Cu(I) site whilst the other contained a five coordinate Cu(II) site. This was the first crystallographic demonstration of the three-coordinate Cu(I) site in bovine CuZnSOD and the first time that both the oxidized and the reduced Cu-site conformations had been observed in the same crystal structure (Hough & Hasnain, 1999). The structure of the catalytic site in one subunit of bovine CuZn superoxide dismutase was also shown to be highly variable by a series of crystal structures at ∼1.7 Å, which were collected from different crystals (Hough *et al.*, 2000). These Cu-site conformations lie between those expected for the Cu(II) and Cu(I) forms of the enzyme. This behaviour is not observed for the second subunit of the dimeric enzyme, which remained in the oxidized, Cu(II), state in all cases. The presence of these intermediate structures in the crystal could indicate a slow reduction of the Cu ion during the crystallization process, ultimately resulting in the breakage of the Cu—His61 bond. Another possibility is that the intermediate structures are the result of photoreduction during crystallographic data collection. This explanation was put forward to explain the mixture of Cu(II) and Cu(I) sites in the crystal structure of the naturally monomeric CuZnSOD from *E. coli* (Pesce *et al.*, 1997) as observed in data collected on the third-generation X-ray ring of the ESRF (Stroppolo *et al.*, 1998).

In order to see if there was variability in the samples and whether photoreduction played a role in our experiments at the second-

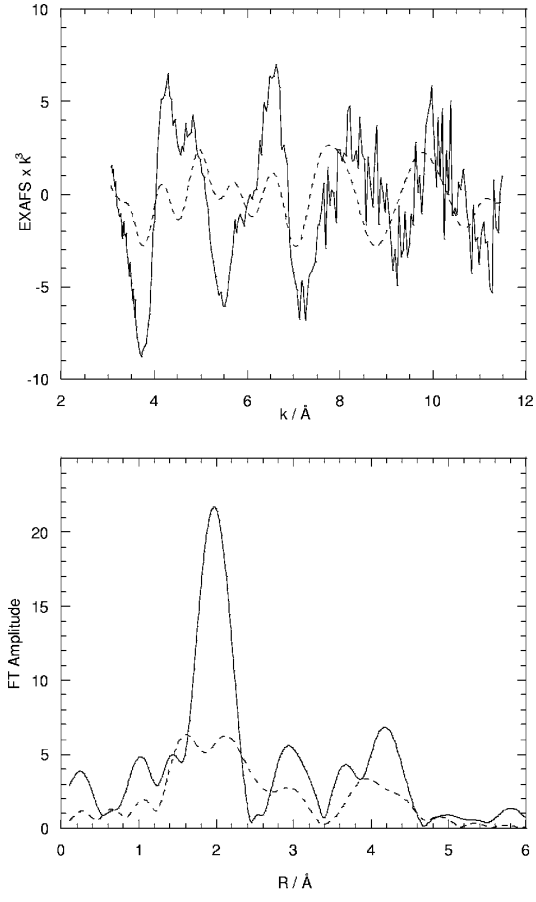

Figure 3
The k^3-weighted *K*-edge EXAFS spectrum of the nitrite-bound type 2 Cu site of AxNiR and a simulation (dashed line) calculated using crystallographic data at 2.8 Å resolution (1NDS.PDB).

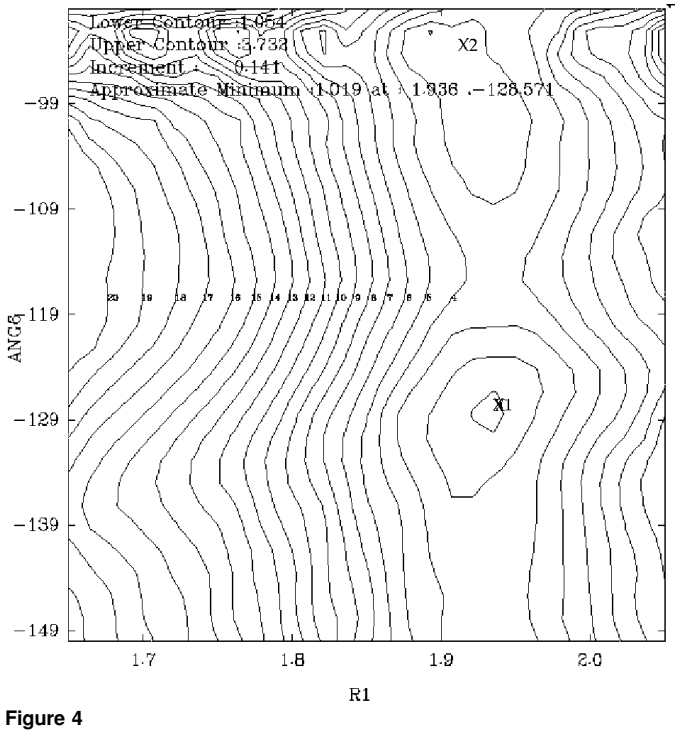

Figure 4
Least-squares contour map of the Cu—O1(nitrite) bond length *versus* the angle Cu—O1(nitrite)—O2(nitrite). Minima occur at a bond length of 1.94 Å and at two different angles, which correspond to Cu—O2(nitrite) distances of 2.98 Å (marked *X*1) and 2.32 Å (marked *X*2).

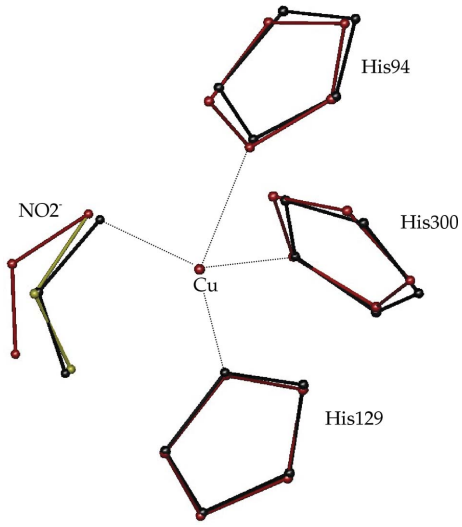

Figure 5
Coordination of the nitrite-bound type 2 Cu site of AxNiR. The crystal structure is shown (black) together with the structures derived from two three-dimensional EXAFS simulations: monodentate (red) and bidentate (green) modes of binding of nitrite to the Cu atom were modelled.

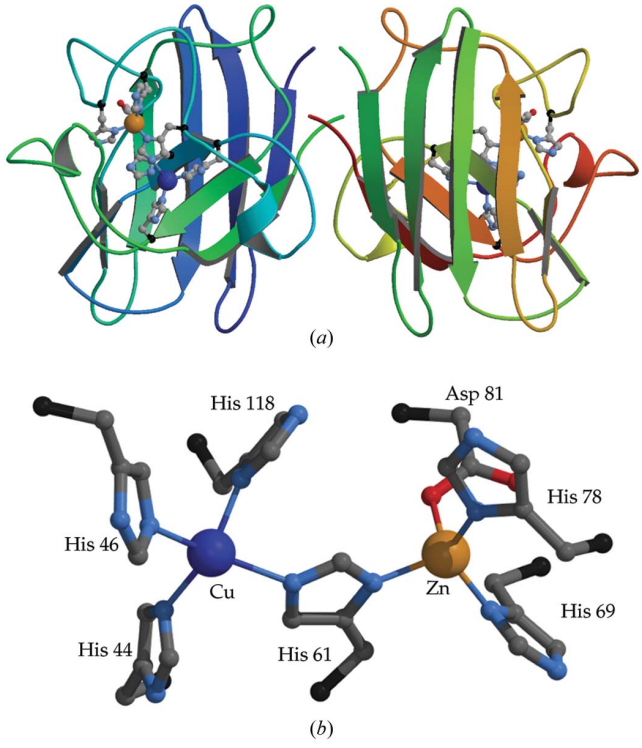

Figure 6
CuZn bovine superoxide dismutase. (*a*) Ribbon diagram of native dimer showing positions of Cu (blue) and Zn (orange) atoms and their ligands and (*b*) a close up of the metal sites and the bridging His61.

generation synchrotron radiation source, the X-ray absorption edges of several crystalline slurry samples were collected at 77 K. These were prepared by crushing crystals grown under 'identical' conditions to those used for the X-ray crystallographic data collection. The experiments were performed with an EXAFS beamline where the photon density is approximately an order of magnitude lower than that of the beamlines used for crystallographic studies, thus there is less scope for photoreduction of Cu. Frozen solution samples of oxidized enzyme do not show any photoreduction at these temperatures and photon dose. A fully oxidized Cu *K*-edge EXAFS spectrum was obtained from one sample of crystalline slurry, as shown in Fig. 7(*a*) where the spectrum is compared with a spectrum measured from a solution of oxidized SOD. The data are essentially identical, with the major absorption (peak *A*) occurring at 8990–9000 eV and with a small pre-edge peak (peak *B*) at ~8982 eV. In Fig. 7(*b*) this spectrum is shown again together with the Cu *K*-edge data for four other crystalline slurry samples. These data show clear variations in the intensity, shape and position of both the major peak *A* and the small pre-edge feature *B*. In particular, peak *B* shows a gradual shift to lower energy compared with the fully oxidized spectrum [see Fig. 7(*c*), left-hand panel]. The XANES of small-molecule analogues of the Cu site of oxidized SOD [*i.e.* systems that contain Cu(II) coordinated by four histidine ligands and one or more axial N or O ligands] have been shown to possess similar pre-edge features that arise from photoelectron

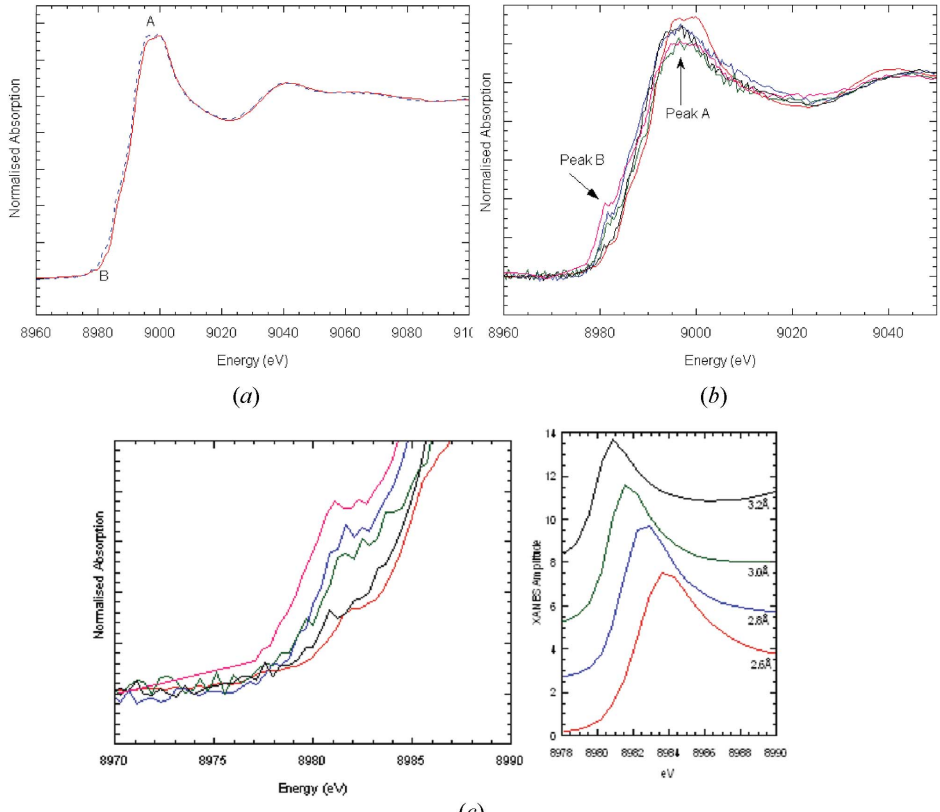

Figure 7
(*a*) XAFS spectrum of a crystalline slurry (dashed line) and a fully oxidized solution spectrum recorded from bovine SOD. (*b*) The XANES of the above spectrum is compared with data for three other crystalline samples and shows clear variation in both peak *A* and peak *B*. (*c*) An expanded view of peak *B* above (left-hand panel) and calculated spectra for varying distances of one of the ligands (right-hand panel).

scattering by the axial ligand(s) (Strange *et al.*, 1990). The position (energy) of this absorption feature depends on the Cu–axial-ligand distance and shifts to lower energy with increasing distance. This effect is seen in Fig. 7(*c*) (right-hand panel), where the variation of the *z*-polarization (axial) component of photoelectron scattering is calculated for a simple model that consists of four N atoms in the *xy* plane (at 2 Å) and one N/O atom along the *z* axis placed at 2.6, 2.8, 3.0 and 3.2 Å. These pre-edge features in Cu(II) complexes are determined by the position (*i.e.* Cu–ligand distance) and type of axial ligand (*e.g.* covalent, ionic) (Kau *et al.*, 1987; Onori *et al.*, 1988). The pre-edge feature that appears in the reduced spectra is ∼2 eV higher in energy than those shown in the slurry spectra. Thus, the changes seen in the absorption edges of the crystalline slurry samples represent a state where the Cu atoms are fully oxidized but where the ligated water molecule is moving further away from the metal.

Recently we obtained atomic-resolution (1.15 Å) data for a fully reduced bovine SOD (Hough & Hasnain, 2003). The details of the metrical information at the Cu sites seen at this resolution are in excellent agreement with the EXAFS results obtained on a frozen solution of the chemically reduced enzyme (Murphy, Strange & Hasnain, 1997). Fig. 8(*a*) shows a simulation of this data using the atomic-resolution crystal coordinates from monomer *A* (monomer *B* is similar). There is sufficient agreement in the overall fit to the EXAFS so that only a limited amount of further refinement is required to improve the simulation. The atomic-resolution coordinates are already very close to the final fit parameters. This is in stark contrast to a simulation of Cu EXAFS of oxidized bovine SOD using 1.65 Å crystal structure parameters (Fig. 8*b*). The Cu–ligand distances are clearly much longer in the crystal structure than those predicted by EXAFS. We anticipate that atomic-resolution data for oxidized SOD will show a much better agreement between the two techniques. This result, and the similar result for nitrite reductase, suggests that crystallographic structure determination should be extended to atomic resolution (or better) whenever possible and that we should not be content with lower resolution if the objective is to understand the detailed chemistry of metal sites in proteins. This work also demonstrates the reliability and value of using the XAFS technique to study metal coordination in proteins when crystal structures are already available.

4. Conclusions

The interplay of BioXAS and high-resolution X-ray crystallography for structure–function studies of metalloproteins is thus clear. The two techniques have natural synergy, and if they are applied together significant advances in our understanding of this important class of proteins can be made. We believe, given the common instrumentation for MAD-based (multiple anomalous scattering) structural genomics programmes and BioXAS (Hasnain & Hodgson, 1999), that routine

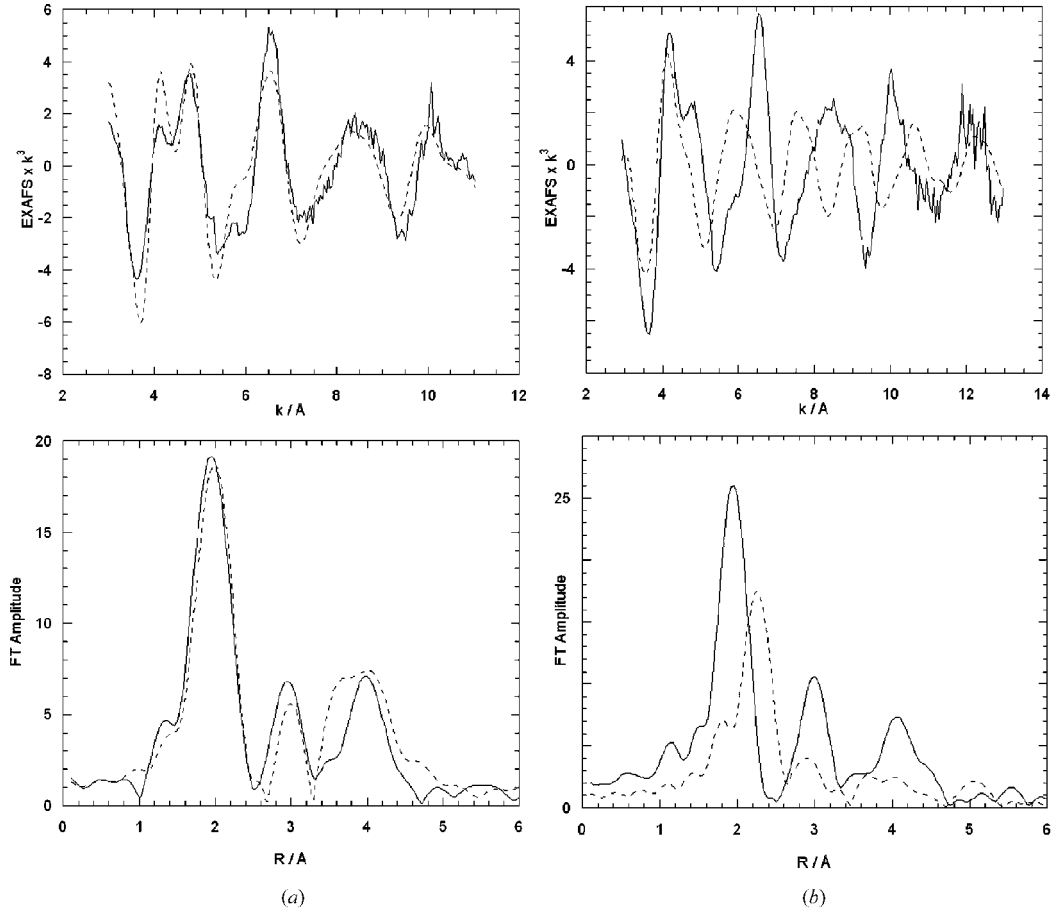

Figure 8
Simulations of Cu *K*-edge EXAFS data from frozen solutions of CuZn bovine SOD. (*a*) The reduced EXAFS, fitted using coordinates from the atomic-resolution (1.15 Å) crystal structure (Hough & Hasnain, 2003), with three histidine ligands coordinated at 1.96, 2.03 and 2.06 Å. (*b*) The oxidized EXAFS using crystal structure coordinates from a 1.65 Å resolution data set, with four histidine ligands and a water molecule at 2.0, 2.15, 2.21, 2.21 and 2.54 Å, respectively (Hough & Hasnain, 1999).

XAS measurements should be undertaken whenever crystallographic data for a structural genomics protein are being collected.

References

Adman, E. T., Godden, J. E. & Turley, S. (1995). *J. Biol. Chem.* **270**, 27458–27474.

Ascone, I., Castamer, R., Bolognesi, M., Tarricone, C., Strappolo, M. E. & Desideri, A. (1997). *Biochem. Biophys. Res. Commun.* **241**, 119–121.

Bertini, I., Luchinat, C., Ming, L. J., Piccoli, M., Sola, M. & Valentine, J. S. (1992). *Inorg. Chem.* **31**, 4433–4435.

Binsted, N., Gurman, S. J., Campbell, J. W. & Stephenson, P. (1991). *SERC Daresbury Laboratory Program EXCURVE.* Daresbury Laboratory, Warrington, UK.

Binsted, N. & Hasnain, S. S. (1996). *J. Synchrotron Rad.* **3**, 185–196.

Binsted, N., Strange, R. W. & Hasnain, S. S. (1992). *Biochemistry*, **31**, 12117–12125.

Blackburn, N. J., Hasnain, S. S., Binsted, N., Diakun, G. P., Garner, C. D. & Knowles, P. F. (1984). *Biochem. J.* **219**, 985–990.

Bordo, D., Djinovic, K. & Bolognesi, M. (1994). *J. Mol. Biol.* **238**, 366–386.

Cheung, K. C., Strange, R. W. & Hasnain, S. S. (2000). *Acta Cryst.* D**56**, 697–704.

Djinovic, K., Gatti, G., Coda, A., Antolini, L., Pelosi, G., Desideri, A., Falconi, M., Marmocchi, F., Rotilio, G. & Bolognesi, M. (1992). *J. Mol. Biol.* **225**, 791–809.

Dodd, F. E., Hasnain, S. S., Abraham, Z. H. L., Eady, R. R. & Smith, B. E. (1997). *Acta Cryst.* D**53**, 406–418.

Dodd, F. E., Van Beeumen, J., Eady, R. R. & Hasnain, S. S. (1998). *J. Mol. Biol.* **282**, 369–382.

Ellis, M. J., Dodd, F. E., Strange, R. W., Prudêncio, M., Sawers, G., Eady, R. R. & Hasnain, S. S. (2001). *Acta Cryst.* D**57**, 1110–1118.

Ellis, M. J., Eady, R. R. & Hasnain, S. S. (2003). *Acta Cryst.* D. In preparation.

Godden, J. W., Turley, S., Teller, D. C., Adman, E. T., Liu, M. Y., Payne, W. J. & LeGall, J. (1991). *Science*, **253**, 438–442.

Hart, P. J., Liu, H., Pellegrini, M., Nersissian, A. M., Gralla, E. B., Valentine, J. S. & Eisenberg, D. (1998). *Protein Sci.* **7**, 545–555.

Hasnain, S. S. & Hodgson, K. O. (1999). *J. Synchrotron Rad.* **6**, 864–875.

Hough, M. & Hasnain, S. S. (1999). *J. Mol. Biol.* **287**, 579–592.

Hough, M. & Hasnain, S. S. (2003). *J. Mol. Biol.* In preparation.

Hough, M. A., Strange, R. W. & Hasnain, S. S. (2000). *J. Mol. Biol.* **304**, 231–241.

Howes, B. D., Abraham, Z. H. L., Lowe, D. J., Brüser, T., Eady, R. R. & Smith, B. E. (1994). *Biochemistry*, **33**, 3171–3177.

Kau, L., Spira-Solomon, D., Penner-Hahn, J. E., Hodgson, K. O. & Solomon, E. I. (1987). *J. Am. Chem. Soc.* **109**, 6433–6442.

Kokimota, M., Nishiyama, M., Murphy, M. E. P., Turley, S., Adman, E. T., Horinuochi, S. & Beppu, T. (1994). *Biochemistry*, **33**, 5246–5252.

McAdam, M. E., Fox, R. A., Lavelle, F. & Fielden, M. F. (1977). *Biochem. J.* **165**, 71–79.

Murphy, L. M., Strange, R. W. & Hasnain, S. S. (1997). *Structure*, **5**, 371–379.

Murphy, M. E. P., Turley, S. & Adman, E. T. (1997). *J. Biol. Chem.* **272**, 28455–28460.

Murphy, M. E. P., Turley, S., Kukimoto, M., Nishiyama, M., Horinouchi, S., Sasaki, H., Tanoruki, M. & Adman, E. T. (1995). *Biochemistry*, **34**, 12107–12117.

Ogihara, N., Parge, H. E., Hart, P. J., Weiss, M. S., Goto, J. J., Crane, B. R., Tsang, J., Slater, K., Roe, J. A., Valentine, J. S., Eisenberg, D. & Tanier, J. A. (1996). *Biochemistry*, **35**, 2316–2321.

Onori, G., Santucci, A., Scafati, A., Belli, M., Della Longa, S., Bianconi, A. & Palladino, L. (1988). *Chem. Phys. Lett.* **149**, 289–293.

Pesce, A., Capasso, C., Battistoni, A., Folcarelli, S., Rotilio, G., Desideri, A. & Bolognesi, M. (1997). *J. Mol. Biol.* **274**, 408–420.

Rypniewski, W. R., Mangani, S., Bruni, B., Orioli, P. L., Casati, M. & Wilson, K. S. (1995) *J. Mol. Biol.* **251**, 282–296.

Strange, R. W., Alagna, L., Durham, P. J. & Hasnain, S. S. (1990). *J. Am. Chem. Soc.* **112**, 4265–4268.

Strange, R. W., Dodd, F. E., Abraham, Z. H. L., Grössmann, J. G., Brüser, T., Eady, R. R., Smith, B. E. & Hasnain, S. S. (1995). *Nature Struct. Biol.* **2**, 287–292.

Strange, R. W., Murphy, L. M., Dodd, F. E., Abraham, Z. H. L., Eady, R. R., Smith, B. E. & Hasnain, S. S. (1999). *J. Mol. Biol.* **287**, 1001–1009.

Stroppolo, M. E., Nuzzo, S., Pesce, A., Rosano, C., Battistoni, A., Bolognesi, M., Mobilio, S. & Desideri, A. (1998). *Biochem. Biophys. Res. Commun.* **249**, 579–582.

Tainer, J. A., Getzoff, E. D., Beem, K. M., Richardson, J. S. & Richardson, D. C. (1982). *J. Mol. Biol.* **160**, 181–217.

Tainer, J. A., Getzoff, E. D., Richardson, J. S. & Richardson, D. C. (1983). *Nature*, **306**, 284–287.

Zumpft, W. G. (1997). *Microbiol. Mol. Biol. Rev.* **61**, 533–616.

Received 23 August 2002 • Accepted 4 December 2002